


Anomalous transition with modulation around band degeneraciesMeng Xiao ^{*}*Key Laboratory of Artificial Micro- and Nano-Structures of Ministry of Education and School of Physics and Technology, Wuhan University, Wuhan 430072, China
and Wuhan Institute of Quantum Technology, Wuhan 430206, China*

(Received 10 September 2022; revised 9 January 2023; accepted 18 April 2023; published 1 May 2023)

A resonance transition occurs between two states when the system is under an oscillatory driving field with a proper frequency. It is commonly believed that frequency must be matched at the resonance transition. Here we show that the above condition is not necessarily satisfied when the system under driving encloses nontrivial band degeneracies, such as a Dirac point. We consider a kagome lattice under the modulation of an artificial gauge field and show the inequivalence of the modulation frequency and energy difference between states at transitions. Meanwhile, our analytical formula reveals that the transitions exhibit chirality around the Dirac cone. When the system Hamiltonian under modulation circles around a higher-order charged band degeneracy, the fundamental one-photon transition is absent. These peculiar properties can be explained with the effective Hamiltonian under n -fold rotational symmetry.

DOI: [10.1103/PhysRevB.107.L180101](https://doi.org/10.1103/PhysRevB.107.L180101)

Conservation of energy and momentum plays crucial roles in various emission or absorption spectroscopies for identifying structural fingerprints, such as Raman spectroscopy [1], electron energy-loss spectroscopy [2], etc. [3]. Generally, frequency and momentum must be matched if one wants to achieve a resonance transition between two states [4–9]. The two states under consideration can be quantum states of atomic systems [7,8], optical states [4–7], electronic states [9], qubits in superconducting circuits [10,11], etc. The modulation which induces the transition needs not be necessarily optically induced. It can also be introduced by a phonon as has been widely implemented in optomechanical cavities [12]. The energy conservation in resonance transition originates from matching the phase factor. Meanwhile, we are also aware that a geometric phase can introduce an additional phase term independent of the dynamical phase [13,14]. Thus, asking how such a geometric phase may modify the resonance transition process when the system Hamiltonian under modulation encloses a nontrivial geometric phase is curious.

There are band degeneracies, such as the two-dimensional (2D) Dirac points possessing nontrivial topological charges and, thus, a nonzero geometric phase around them. Here I show that such topological band degeneracies play vital roles in a resonance transition process especially when the system Hamiltonian is modulated to circle them. Under this condition, the maximum transition amplitude occurs at a modulation frequency (denoted by Ω_p) which is not solely determined by the frequency (energy) difference between two states. The analytical solutions show that Ω_p derives from the energy difference by the modulation strength (up to a constant). Meanwhile, Ω_p exhibits a linear dependence on the mass term that lifts the Dirac point degeneracy. In return, Ω_p can be utilized to measure this effective mass.

Consider a two-level system and assume the system initially only populates the lower-energy state as sketched in Fig. 1(a). The system is modulated by either an incident optical wave (photon) or a mechanical oscillation (phonon) with a modulation frequency Ω . In general, a resonance transition is achieved when the energy difference of these two states is multiple times the modulation frequency, i.e.,

$$\Delta E = m\Omega_p, \quad (1)$$

where $m \in \mathbb{Z}^+$. $m > 1$ represents the multiphoton (phonon) process. To derive Eq. (1), one needs to assume that the modulation can be treated as a perturbation where the system Hamiltonian does not change much in the presence of the modulation. This assumption is generally true for the vast majority of scenarios, and, thus, Eq. (1) works for almost all the known cases.

Exceptional cases exist where Eq. (1) does not hold, say, when the system Hamiltonian under modulation involves singular points. The evolution path can enclose the singular points, and the impacts of these singular points can still be observed. Figure 1(b) provides one such example wherein the singular point's impact must be considered. Here I consider a three-level system where the two excited energy levels form a conical dispersion (2D Dirac cone). It is known that any states, electric or photonic, located on the Dirac cone will experience a Berry phase π whereas circulating the Dirac point [15–17]. The modification of energy spectra due to the Berry phase in the adiabatic limit is well studied [18–20]. However, how it affects the nonadiabatic resonance transition process remains unexplored. The system under modulation evolves along a predefined path as highlighted by the yellow circle with modulation strength and frequency given by δ_A and Ω , respectively. δ_A is assumed to be a small number, and, hence, the energy of the lowest band can be approximated by a constant and the Dirac cone by a linear dispersion. Under such an evolution path, the energy differences between the lowest

^{*}phmxiao@whu.edu.cn

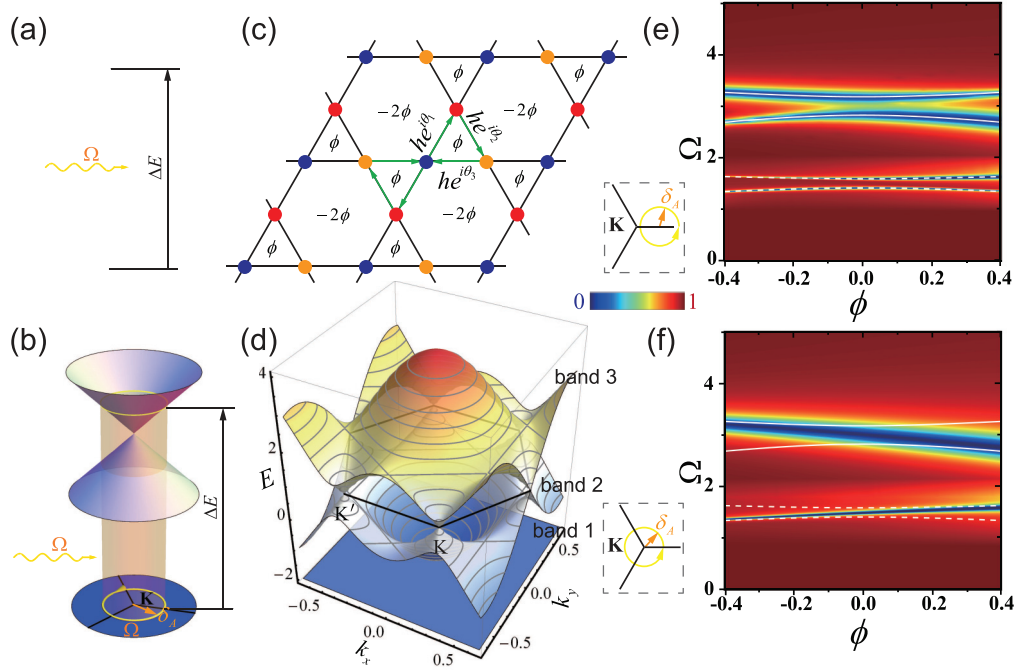


FIG. 1. (a) A system is excited from a lower-energy state to a higher-energy state with a modulation frequency Ω . (b) Similar as (a) but the higher two levels now exhibit a conical dispersion. (c) A kagome lattice with a nonvanishing local magnetic flux. Here the green arrows denote the positive hopping phase direction, and colored disks denote different sublattices. (d) The band structure of the kagome lattice in (c) with $\phi = 0$, which exhibits a flat band and a conical dispersion at the K and K' points. (e) and (f) The minimal amplitude of wave function remains on band 1 as a function of the modulation frequency Ω and the magnetic flux ϕ . The lower left insets in (e) and (f) sketch the corresponding modulation profiles. Here the solid white line shows the energy difference among bands 2, 3, and 1, and the dashed white lines are halves of the energy differences. $\delta_A = 0.15$ and the circling center \vec{k}_c is at $2\pi(1, \sqrt{3})/3 + (0.2, 0)$ for (e). $\delta_A = 0.2$ and \vec{k}_c is at the K point in (f).

band and the excited states remain constant, simplifying the situation. Thus, one would expect two explicit values of Ω at which the lowest band reaches resonance with the higher bands as indicated by Eq. (1). However, as will be shown later, Eq. (1) does not hold for the case in Fig. 1(b).

I consider a kagome lattice as shown in Fig. 1(c) [21–23]. To achieve the modulation presented in Fig. 1(b), I include a uniform vector potential given by

$$\vec{A}(t) = \delta_A [\cos(\Omega t)\hat{x} + \sin(\Omega t)\hat{y}]. \quad (2)$$

Meanwhile, I added a nonuniform magnetic flux that can lift the Dirac cone degeneracy for later purposes. Here the red, blue, and orange disks represent three sublattices, and the green arrows denote the directions of positive phase hopping. According to the Peierls substitution [24,25], $\theta_1 + \theta_2 + \theta_3 = \phi$ and for simplicity, we set $\theta_{1-3} = \phi/3$ and the hopping amplitude $h \equiv 1$. The possible realizations are discussed at the end. Also, until otherwise specified, we set the charge of electron $e = 1$ and $\hbar = 1$ throughout this Letter; hence, the gauge potential shares the same unit as the wave vector. The Hamiltonian of this system is given by

$$\hat{H} = \begin{pmatrix} 0 & 2e^{i\theta_1} \cos[(\vec{k} + \vec{A}) \cdot \vec{r}_1] & 2e^{-i\theta_3} \cos[(\vec{k} + \vec{A}) \cdot \vec{r}_3] \\ 2e^{-i\theta_1} \cos[(\vec{k} + \vec{A}) \cdot \vec{r}_1] & 0 & 2e^{i\theta_2} \cos[(\vec{k} + \vec{A}) \cdot \vec{r}_2] \\ 2e^{i\theta_3} \cos[(\vec{k} + \vec{A}) \cdot \vec{r}_3] & 2e^{-i\theta_2} \cos[(\vec{k} + \vec{A}) \cdot \vec{r}_2] & 0 \end{pmatrix}, \quad (3)$$

where $\vec{r}_1 = (1, \sqrt{3})/4$, $\vec{r}_2 = (1, -\sqrt{3})/4$ and $\vec{r}_3 = (-1, 0)/2$. Here for simplicity, the dependence of \hat{H} and \vec{A} on time (t) are not given explicitly. The equation that governs the system dynamics is

$$i \frac{\partial}{\partial t} |\psi(t)\rangle = \hat{H} |\psi(t)\rangle. \quad (4)$$

The band structure when $\delta_A = 0$ (modulation is off) and $\phi = 0$ is provided in Fig. 1(d), which exhibits the band

dispersion needed in Fig. 1(b) near the $K = 2\pi(1, \sqrt{3})/3$ point. The \vec{A} field I introduced shifts the kinetic momentum and, thus, raises the circling modulation. Here the perfect flatness of the lowest band presented for the kagome lattice is not necessary, but it does simplify the discussion.

Then I proceed to turn on the modulation. When the modulation frequency Ω is small, the system evolves adiabatically, and one can easily identify the Berry phase possessed by the

TABLE I. List of resonance transitions. The second column labels initial band number \rightarrow excited band number. The third column gives the corresponding coupling term, where “ \oplus ” represents a two-photon process. The rightmost column labels the modulation frequency at the resonance transition.

Peaks	Transitions	Coupling term	Peak modulation frequency
Primary peak 1	band 1 \rightarrow band 3	H_{31}^K	$\Omega_{p1} = -3 - \phi/\sqrt{3} + 3\delta_A^2/16$
Primary peak 2	band 1 \rightarrow band 2	H_{12}^K	$\Omega_{p1} = 3 - \phi/\sqrt{3} - 3\delta_A^2/16$
Secondary peak 1	band 1 \rightarrow band 3	$H_{12}^K \oplus H_{23}^K$	$\Omega_{p2} = 1.5 + \phi/2\sqrt{3} - 3\delta_A^2/32$
Secondary peak 2	band 1 \rightarrow band 2	$H_{13}^K \oplus H_{32}^K$	$\Omega_{p2} = -1.5 + \phi/2\sqrt{3} + 3\delta_A^2/32$

Dirac cone. As Ω increases, field amplitudes oscillate between different bands, similar to a complex version of Rabi oscillation. I first set the wave-vector \vec{k} at $\vec{k}_c = K + (0.2, 0)$ and $\delta_A = 0.15$ as a control example where Eq. (1) is satisfied. Here the Dirac cone is not enclosed by the circling path as sketched by the lower-left inset in Fig. 1(e). Initially, ($t = 0$) only the lowest band is populated, i.e., $|\psi(0)\rangle = |v_1(0)\rangle$, where $|v_i(t)\rangle$ with $i \in \{1-3\}$ represent the instantaneous eigenstates of the system Hamiltonian. To characterize the transition probability to higher bands, I record the minimum remaining amplitude at the lowest state, i.e., $\min_t |\langle \psi(t) | v_1(t) \rangle|$. It as a function of the modulation frequency Ω and flux ϕ is shown in Fig. 1(e). Note here that the dependence of instantaneous eigenstates on t is introduced as the Hamiltonian in Eq. (3) is time dependent (not due to the dynamical phase, which is irrelevant for our observation). For most sets of Ω and ϕ , the ground state cannot be excited (the color remains red). There are four prominent canyons (two roughly $\Omega \approx 3$ and the other two $\Omega \approx 1.5$) where the ground states can be excited to higher bands. The narrower canyon is almost at a half modulation frequency of the broader one, which indicates that it comes from a two-photon process. I also provide the time-average energy difference between bands during the circling with the white lines in Fig. 1(e). As expected, the modulation frequencies

at canyons match the average energy difference for both the one-photon and the two-photon processes.

The situation becomes different when the circling path is centered at the K point, i.e., $\vec{k}_c = K = 2\pi(1, \sqrt{3})/3$. Figure 1(f) shows the excitation spectrum with $\delta_A = 0.2$ where the average energy difference is the same as Fig. 1(e). Different from Fig. 1(e), Fig. 1(f) shows only two prominent canyons—one at around $\Omega_{p1} \approx 3$ for the one-photon process and the other roughly $\Omega_{p2} \approx 1.5$ for the two-photon process. Meanwhile, as δ_A is small, the band is almost isotropic, and the energy difference is negligibly small along the circling path. Thus, obviously, the modulation frequencies at the canyons do not match either energy difference between those bands [white lines in Fig. 1(f)]. In other words, an apparent inconsistency emerges as the Dirac cone is enclosed in the circling path.

To understand this inconsistency, I derive the effective Hamiltonian which describes the system under modulation. For small δ_A , the system's dynamics can be captured by the effective Hamiltonian around the K point. We expand the Hamiltonian in Eq. (3), and perform a unitary transformation such that the coupling terms appear off-diagonal. When $\vec{k}_c = K$, the effective Hamiltonian is given by

$$H^K = \begin{pmatrix} -2 + \frac{\delta_A^2}{8} & \frac{1}{4}e^{i(\Omega t + \pi/6)}\delta_A(\sqrt{3} + \phi) & \frac{1}{4}e^{-i(\Omega t + \pi/6)}\delta_A(\sqrt{3} - \phi) \\ \frac{1}{4}e^{-i(\Omega t + \pi/6)}\delta_A(\sqrt{3} + \phi) & 1 - \frac{\phi}{\sqrt{3}} - \frac{\delta_A^2}{16} & \frac{\sqrt{3}}{2}e^{i(\Omega t - \pi/3)}\delta_A \\ \frac{1}{4}e^{i(\Omega t + \pi/6)}\delta_A(\sqrt{3} - \phi) & \frac{\sqrt{3}}{2}e^{-i(\Omega t - \pi/3)}\delta_A & 1 + \frac{\phi}{\sqrt{3}} - \frac{\delta_A^2}{16} \end{pmatrix}. \quad (5)$$

Distinctly different from other resonance transitions [say, Fig. 1(e)], here the energy difference between diagonal terms ($3 \pm \phi/\sqrt{3} - 3\delta_A^2/16$) do not equal the energy difference between the ground and the excited states ($3 \pm \sqrt{\phi^2/3 + 3\delta_A^2/2}$). This explains why the canyons do not match the white lines in Fig. 1(f). Meanwhile, the off-diagonal coupling terms originate from modulation exhibit definite chirality. (Only positive or negative frequency is allowed for each transition). From the effective Hamiltonian in Eq. (5), we can identify four possible resonance transition processes, two with positive Ω_p and the other two with negative Ω_p as listed in Table I. The two primary (secondary) peaks come from one-photon (two-photon) processes. On the rightmost column, we also provide the modulation frequencies at which the system reaches resonance transition. Choose the primary

peak 1 as an example, $\Omega_{p1} = -3 - \phi/\sqrt{3}$, which corresponds to resonance transition from H_{11}^K to H_{33}^K with modulation term $H_{31}^K = e^{-i(\Omega t + \pi/6)}\delta_A(\sqrt{3} - \phi)/4$. We can see only two transition processes for positive Ω which is consistent with Fig. 1(f). More intriguingly, the above statement is true in the $\delta_A \rightarrow 0$ limit (independent of δ_A) where positive (negative) Ω_{p1} couples only to the lower (higher) excited state. Note here $\phi/\sqrt{3}$ gives the effective mass at the valley, and, thus, the effective mass near the band edge can be obtained through the opposite dependence of the primary and secondary peaks on ϕ .

I proceed to supplement the theoretical predictions in Table I with numerical simulations. First, I set $\phi = 0$ and $|\psi(0)\rangle = |v_1(0)\rangle$. The maximum probability of finding a state on band 3, i.e., $\max_t |\langle \psi(t) | v_3(t) \rangle|^2$, as functions of δ_A and Ω is shown in Fig. 2(a). There are two primary

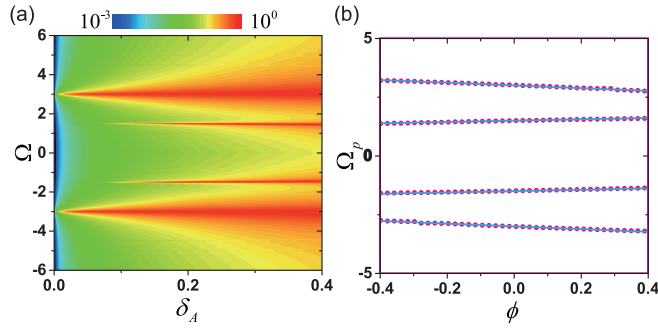


FIG. 2. (a) The maximum probability of finding a state on band 3 (color code) around the K point as a function of the modulation strength δ_A and the modulation frequency Ω . (b) Modulation frequency at resonance transition Ω_p as a function of the magnetic flux ϕ . The solid magenta disks are extracted from the numerical simulations, and the blue lines are analytical results from Table I. Here I set $|\psi(0)\rangle = |v_1(0)\rangle$ and \vec{k}_c is at the K point for both (a) and (b), $\phi = 0$ in (a), and $\delta_A = 0.2$ in (b).

peaks located at $\Omega_{p1} = \pm 3$ and two other secondary peaks located at $\Omega_{p2} = \pm 1.5$ whose maximum are independent of δ_A as predicted. The peaks broaden with the increasing of δ_A . The full width at half maximum (FWHM) is fitted to be $1.776\delta_A$ ($0.453\delta_A^2$) for the two primary (secondary) peaks. (See Sec. I in the Supplemental

Material of Ref. [26] for more details [18–20,27–33].) The linear (quadratic) dependence on δ_A for the primary (secondary) peaks confirms that it is a one-photon (two-photon) process. According to the Rabi model, a one-photon process should exhibit an FWHM of $\sqrt{3}\delta_A$ when $\phi = 0$, which is reasonably close to $1.776\delta_A$ as a first-order approximation. Second, I fix $\delta_A = 0.2$ and numerically investigate the dependence of Ω_p on ϕ . The results are shown with magenta dots in Fig. 2(b). Meanwhile, the analytical solutions in the rightmost column of Table I are also provided with blue lines, which agree reasonably well with the numerical simulations.

A Dirac point is a band degeneracy that exhibits the lowest-order topological singularity, and there are also other higher-order charged band degeneracies. With the same Hamiltonian in Eq. (3) at $\phi = 0$, the lower two bands at Γ consist of a degeneracy with a Berry phase of 2π . At any nonzero ϕ , this degeneracy is lifted. As before, I set $|\psi(0)\rangle = |v_1(0)\rangle$. For the modulation, I set $\vec{k}_c = \Gamma$ and \vec{A} is still given by Eq. (2) as sketched in Fig. 3(a). The maximum probability of finding a state on the highest band, $\max_t |\langle \psi(t) | v_3(t) \rangle|^2$ at $\delta_A = 1$ is shown in Fig. 3(b). We can see two primary peaks located at $\Omega_{p1} \approx \pm 2.8$ and two secondary peaks at $\Omega_{p2} \approx \pm 1.4$. At $\delta_A = 1$, the energy difference between band 1 and band 3 is 5.625, indicating the absence of the fundamental transition $\Omega_p \approx \Delta E$ for such a modulation scheme.

To unveil the underline physics, I derive the effective Hamiltonian,

$$H^\Gamma = \begin{pmatrix} (-2 + \delta_A^2/8)(1 - \phi/\sqrt{3}) & -e^{-2i\Omega t} \delta_A^2/8 & -e^{-2i\Omega t} \delta_A^2(1 + \phi/\sqrt{3})/16 \\ -e^{2i\Omega t} \delta_A^2/8 & (-2 + \delta_A^2/8)(1 + \phi/\sqrt{3}) & -e^{-2i\Omega t} \delta_A^2(1 - \phi/\sqrt{3})/16 \\ -e^{-2i\Omega t} \delta_A^2(1 + \phi/\sqrt{3})/16 & -e^{2i\Omega t} \delta_A^2(1 - \phi/\sqrt{3})/16 & 4 - \delta_A^2/4 \end{pmatrix}. \quad (6)$$

One distinct difference from Eq. (5) is that the off-diagonal coupling term is $\exp(\pm 2i\Omega t)$ instead of $\exp(\pm i\Omega t)$, although the modulation frequency is still Ω . According to the effective Hamiltonian at the Γ point (H^Γ), there should be only two possible resonance transitions between bands 1 and 3. However, due to the near degeneracy at Γ , states switch rapidly between bands 1 and 2 during the circling process. As a result, one can also observe another two resonance transitions between bands 2 and 3, although initially, only band 1 is excited. Hence, following the analysis above, Ω_p as functions of ϕ for the major and secondary peaks are given by

$$\Omega_{p1} = \pm \left(3 - \frac{3}{16} \delta_A^2 \right) - \phi/\sqrt{3}, \quad (7a)$$

and

$$\Omega_{p2} = \pm \left(\frac{3}{2} - \frac{3}{16} \delta_A^2 \right) + \phi/2\sqrt{3}, \quad (7b)$$

respectively. The analytical relations in Eq. (7) are also provided in Fig. 3(b) with the gray dashed lines, which perfectly explain the numerical simulations. Note here the energy difference between the lower two bands and band 3 is

$$\Delta E = 3 - \frac{3}{16} \delta_A^2 \pm \sqrt{\frac{1}{64} \delta_A^4 + \frac{4}{3} \phi^2}. \quad (8)$$

Thus, Eq. (1) is still not satisfied under such a modulation scheme. Above, I use the kagome lattice as an example to illustrate the peculiar behaviors. In Secs. II and III in the Supplemental Material of Ref. [26], I analyze the modulation around the Dirac cone in the graphene lattice and

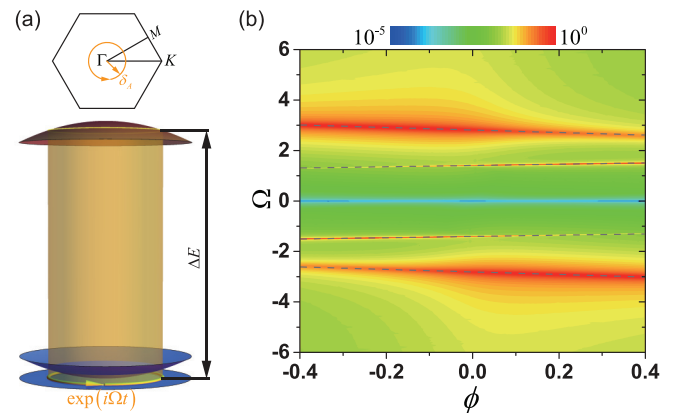


FIG. 3. (a) A sketch shows a modulation scheme around the Γ point. (b) The maximum probability of finding a state on band 3 (color code) as a function of the modulation frequency Ω and the magnetic flux ϕ . Here I set $|\psi(0)\rangle = |v_1(0)\rangle$ and $\delta_A = 1$.

around the double Dirac cone in the shrunk graphene lattice at the Γ point. For the graphene lattice, we can still see the off-diagonal chiral transition term. Meanwhile, for the modulation around the double Dirac cone, I find that the fundamental transition $\Omega_p \approx \Delta E$ appears for the shrunk graphene. Thus, the absence of a fundamental transition process $\Omega_p \approx \Delta E$ is a unique feature for H^Γ in the kagome lattice. To unveil which feature is tied to the specific model, I analyze the requirements on the effective Hamiltonian as enforced by the n -fold rotational symmetry ($n \in \{2-4, 6\}$) in the Supplemental Material of Ref. [26]. The results are summarized in Table S1 of the Supplemental Material of Ref. [26]. It shows that the off-diagonal chiral transition terms are generally presented in systems with n -fold rotational symmetry. The specific form of the off-diagonal chiral transition, i.e., $\delta_A^m \exp(\pm im\Omega t)$ with $m \in \{1-3\}$, depends solely on the ratio of the rotational eigenvalues between the two bands under consideration. Meanwhile, the effective Hamiltonian also reveals that Ω_p should be generally different from the energy difference between these two bands. Previous works had shown the shift of resonance frequency [18,29,31] and the change of the transition probability [30,32] due to the presence of the Berry phase. However, the underline mechanisms are fundamentally different from our Letter. (See a detailed discussion in Sec. V in the Supplemental Material of Ref. [26].)

The systems discussed herein should be implementable with the state-of-the-art technique. The kagome lattice has already been fabricated and studied in photonic crystals, cold atoms, and electronic systems [22,34–36]. In photonic systems, the vector potential $\vec{A}(t)$ (including the local magnetic flux potential) can be introduced by dynamical modulations

where the hopping phase between two lattice sites can be arbitrarily tuned [4,37,38]. $\vec{A}(t)$ generated with dynamical modulation has also been confirmed experimentally [39,40]. In cold atoms, $\vec{A}(t)$ can be realized with an effective electric field that has already been demonstrated experimentally [41,42]. In electronic systems, $\vec{A}(t)$ can be introduced by a circularly polarized light [43–45].

To summarize, this Letter shows that if the system under modulation evolves around topologically charged band degeneracies with nonzero geometric phases, the energy conservation condition needs to be modified. I derive the relation between the modulation frequency at resonance and the mass term which lifts the degeneracy. Off-resonance transitions are routinely used in quantum information processing for preparing or manipulating quantum states [46,47]. Here the resonance transitions under modulation in our Letter provides new insights for identifying structure fingerprint and measuring elementary parameters. As discussed in Sec. VI in the Supplemental Material of Ref. [26], the band structure of a kagome lattice is not a necessity, and the phenomena discussed herein can be observed in diverse systems exhibiting n -fold rotational symmetry. The observations in our Letter can be verified experimentally in photonics, cold atoms, and electronic systems with state-of-the-art techniques.

This work was supported by the National Natural Science Foundation of China (Grant No. 12274332) and the National Key Research and Development Program of China (Grant No. 2022YFA1404900). I thank L. Fang for proofreading and preparing some figures.

I declare no competing financial interests.

-
- [1] C. Raman, *Indian J. Phys.* **2**, 387 (1927).
 [2] J. Hillier and R. F. Baker, *J. Appl. Phys.* **15**, 663 (1944).
 [3] J. C. Lindon, G. E. Tranter, and J. L. Holmes, *Encyclopedia of Spectroscopy and Spectrometry: O-Z* (Academic, San Diego, 2000).
 [4] Z. Yu and S. Fan, *Nat. Photonics.* **3**, 91 (2009).
 [5] J. N. Winn, S. Fan, J. D. Joannopoulos, and E. P. Ippen, *Phys. Rev. B* **59**, 1551 (1999).
 [6] S. T. Cundiff, J. Ye, and J. L. Hall, *Rev. Sci. Instrum.* **72**, 3749 (2001).
 [7] A. Yariv and P. Yeh, *Photonics: Optical Electronics in Modern Communications* (Oxford University Press, Oxford, 2007).
 [8] M. O. Scully and M. S. Zubairy, *Quantum Optics* (Cambridge University Press, Cambridge, UK, 1997).
 [9] C. Kittel, *Introduction to Solid State Physics* (Wiley, Hoboken, NJ, 2004).
 [10] Z.-L. Xiang, S. Ashhab, J. Q. You, and F. Nori, *Rev. Mod. Phys.* **85**, 623 (2013).
 [11] M. H. Devoret and R. J. Schoelkopf, *Science* **339**, 1169 (2013).
 [12] M. Aspelmeyer, T. J. Kippenberg, and F. Marquardt, *Rev. Mod. Phys.* **86**, 1391 (2014).
 [13] S. Pancharatnam, *Proc. Indian Acad. Sci., Sect. A* **44**, 16 (1956).
 [14] M. V. Berry, *Proc. R. Soc. London, Ser. A* **392**, 45 (1984).
 [15] A. H. Castro Neto, F. Guinea, N. M. R. Peres, K. S. Novoselov, and A. K. Geim, *Rev. Mod. Phys.* **81**, 109 (2009).
 [16] S. Raghu and F. D. M. Haldane, *Phys. Rev. A* **78**, 033834 (2008).
 [17] F. D. M. Haldane and S. Raghu, *Phys. Rev. Lett.* **100**, 013904 (2008).
 [18] F. Ghahari *et al.*, *Science* **356**, 845 (2017).
 [19] A. Srivastava and A. Imamoğlu, *Phys. Rev. Lett.* **115**, 166802 (2015).
 [20] J. Zhou, W.-Y. Shan, W. Yao, and D. Xiao, *Phys. Rev. Lett.* **115**, 166803 (2015).
 [21] V. Elser, *Phys. Rev. Lett.* **62**, 2405 (1989).
 [22] A. Mielke, *J. Phys. A* **24**, L73 (1991).
 [23] H. M. Guo and M. Franz, *Phys. Rev. B* **80**, 113102 (2009).
 [24] R. E. Peierls, *Z. Phys.* **80**, 763 (1933).
 [25] D. R. Hofstadter, *Phys. Rev. B* **14**, 2239 (1976).
 [26] See Supplemental Material at <http://link.aps.org/supplemental/10.1103/PhysRevB.107.L180101> for more details, which includes Refs. [18–20,27–33].
 [27] L.-H. Wu and X. Hu, *Phys. Rev. Lett.* **114**, 223901 (2015).
 [28] C. Fang, M. J. Gilbert, X. Dai, and B. A. Bernevig, *Phys. Rev. Lett.* **108**, 266802 (2012).
 [29] K. Toriyama, A. Oguchi, and A. Morinaga, *Phys. Rev. A* **84**, 062103 (2011).

- [30] J. W. Zwanziger, S. P. Rucker, and G. C. Chingas, *Phys. Rev. A* **43**, 3232 (1991).
- [31] D. Xiao, M.-C. Chang, and Q. Niu, *Rev. Mod. Phys.* **82**, 1959 (2010).
- [32] M. V. Berry, Proc. R. Soc. London. Ser. A: Math. Phys. Sci. **430**, 405 (1990).
- [33] A. Dykhne, Sov. Phys. JETP **14**, 1 (1962).
- [34] A. Mielke, *J. Phys. A* **24**, 3311 (1991).
- [35] G.-B. Jo, J. Guzman, C. K. Thomas, P. Hosur, A. Vishwanath, and D. M. Stamper-Kurn, *Phys. Rev. Lett.* **108**, 045305 (2012).
- [36] Y. Zong, S. Xia, L. Tang, D. Song, Y. Hu, Y. Pei, J. Su, Y. Li, and Z. Chen, *Opt. Express* **24**, 8877 (2016).
- [37] K. Fang, Z. Yu, and S. Fan, *Phys. Rev. Lett.* **108**, 153901 (2012).
- [38] K. Fang, Z. Yu, and S. Fan, *Nat. Photonics*. **6**, 782 (2012).
- [39] L. D. Tzuang, K. Fang, P. Nussenzveig, S. Fan, and M. Lipson, *Nat. Photonics* **8**, 701 (2014).
- [40] E. Li, B. J. Eggleton, K. Fang, and S. Fan, *Nat. Commun.* **5**, 3225 (2014).
- [41] N. Fläschner, B. S. Rem, M. Tamowski, D. Vogel, D. S. Lühmann, K. Sengstock, and C. Weitenberg, *Science* **352**, 1091 (2016).
- [42] M. Aidelsburger, M. Lohse, C. Schweizer, M. Atala, J. T. Barreiro, S. Nascimbene, N. R. Cooper, I. Bloch, and N. Goldman, *Nat. Phys.* **11**, 162 (2014).
- [43] W. V. Houston, *Phys. Rev.* **57**, 184 (1940).
- [44] S. A. Oliaei Motlagh, F. Nematollahi, V. Apalkov, and M. I. Stockman, *Phys. Rev. B* **100**, 115431 (2019).
- [45] S. A. Oliaei Motlagh, J.-S. Wu, V. Apalkov, and M. I. Stockman, *Phys. Rev. B* **98**, 081406(R) (2018).
- [46] L. Viola and S. Lloyd, *Phys. Rev. A* **58**, 2733 (1998).
- [47] T. Albash and D. A. Lidar, *Rev. Mod. Phys.* **90**, 015002 (2018).